



OPEN ACCESS

EDITED BY

Julio Sheinbaum,
Centro de Investigación Científica y de
Educación Superior de Ensenada
(CICESE), Mexico

REVIEWED BY

Heriberto Vazquez,
University of California, San Diego,
United States
Gabriela Athié,
Universidad de Veracruz, Mexico

*CORRESPONDENCE

Nektaria Ntaganou
✉ nntaganou@fsu.edu

†PRESENT ADDRESS

Nektaria Ntaganou,
Center for Ocean-Atmospheric
Prediction Studies, Florida State
University, Tallahassee, FL, United States

SPECIALTY SECTION

This article was submitted to
Physical Oceanography,
a section of the journal
Frontiers in Marine Science

RECEIVED 03 June 2022

ACCEPTED 13 January 2023

PUBLISHED 27 January 2023

CITATION

Ntaganou N, Kourafalou V, Beron-Vera FJ,
Olascoaga MJ, Le Hénaff M and
Androulidakis Y (2023) Influence of
Caribbean eddies on the Loop current
system evolution.
Front. Mar. Sci. 10:961058.
doi: 10.3389/fmars.2023.961058

COPYRIGHT

© 2023 Ntaganou, Kourafalou, Beron-Vera,
Olascoaga, Le Hénaff and Androulidakis. This
is an open-access article distributed under
the terms of the [Creative Commons
Attribution License \(CC BY\)](https://creativecommons.org/licenses/by/4.0/). The use,
distribution or reproduction in other
forums is permitted, provided the original
author(s) and the copyright owner(s) are
credited and that the original publication in
this journal is cited, in accordance with
accepted academic practice. No use,
distribution or reproduction is permitted
which does not comply with these terms.

Influence of Caribbean eddies on the Loop current system evolution

Nektaria Ntaganou ^{1*†}, Vassiliki Kourafalou¹,
Francisco Javier Beron-Vera¹, Maria Josefina Olascoaga¹,
Matthieu Le Hénaff^{2,3} and Yannis Androulidakis^{1,4}

¹Department of Ocean Sciences, Rosenstiel School of Marine, Atmospheric, and Earth Science, University of Miami, Miami, FL, United States, ²Cooperative Institute for Marine and Atmospheric Studies (CIMAS), University of Miami, Miami, FL, United States, ³Atlantic Oceanographic and Meteorological Laboratory (AOML), NOAA, Miami, FL, United States, ⁴Department of Civil Engineering, Laboratory of Maritime Engineering and Maritime Works, Aristotle University of Thessaloniki, Thessaloniki, Greece

The Loop Current (LC) system dynamics are an essential component of the processes influencing circulation and transport in the Gulf of Mexico (GoM). The LC evolution is influenced by various factors, including the rich eddy field of the region and the flow exchange through the Yucatan Strait with the neighboring Caribbean Sea. These factors contribute to the complexity of the LC and, as a result, to the limitations in the predictability of the system. The focus of this study is to further elucidate the evolution of the LC, by quantifying the influence of coherent eddy fluxes originating in the Caribbean Sea. This is achieved by employing the Lagrangian-Averaged Vorticity Deviation (LAVD) method, an objective metric to evaluate eddy coherence in the Caribbean Sea that allows, for the first time, to quantify at different depths the evolution of coherent Caribbean eddies through the Yucatan Channel towards the GoM. The physical connectivity between the Caribbean Sea and the GoM is addressed using Lagrangian techniques to analyze processes that take place south of the Yucatan Channel and help quantify their strong relationship with the GoM eddy field. Coherent anticyclonic vorticity fluxes, as well as the net coherent anticyclonic volume transport between the Caribbean Sea and the GoM are associated with Loop Current Eddy (LCE) detachments through direct connectivity between the coherent Caribbean anticyclones and the forming LCE. The findings have important implications for understanding and predicting the LC system and the physical connectivity processes between the GoM and the Caribbean Sea.

KEYWORDS

Lagrangian-Averaged Vorticity Deviation, eddy detection and tracking, HYCOM, Gulf of Mexico, Yucatan Channel

1 Introduction

Understanding and predicting the Loop Current (LC) variability in the Gulf of Mexico (GoM) has been an ongoing effort, mainly due to the rich eddy field of the region (Androulidakis et al., 2014; Le Hénaff et al., 2014) and the irregular behavior of the Loop Current Eddy (LCE) shedding cycles (Vukovich and Maul, 1985; Lugo-Fernández, 2007). Many studies have focused on the processes that take place within the GoM interior and are

tied to the LCE shedding events, such as the intensification and baroclinic instability of frontal cyclones (Schmitz, 2005; Chérubin et al., 2006; Le Hénaff et al., 2012; Donohue et al., 2016). Others have investigated processes in the Caribbean Sea connected to the variability of the LC system, such as wind effects and eddy influence (Oey et al., 2003; Athié et al., 2012; Androulidakis et al., 2021), as well as vorticity flux through the Yucatan Channel (Candela et al., 2002; Oey, 2004; Androulidakis et al., 2021).

In this study, we aim to investigate how the mesoscale eddy field in the northwestern Caribbean Sea may contribute to the LC evolution. We approach the problem by focusing on the interaction between the dominant processes in the GoM (namely LC phase transition from extended to retracted through LCE shedding events) and eddies that originate in the Caribbean Sea and pass through the Yucatan Channel. The effects of Caribbean eddies on the LC variability have not been studied as extensively as the processes that take place in the GoM interior. However, previous studies have shown the importance of including the processes upstream (south of the Yucatan Channel) to further understand the GoM dynamics. The recent study by Androulidakis et al. (2021) showed that the anticyclonic relative vorticity south of the Yucatan Channel is correlated to the eastward tilt of the LC axis and associated with the eastward shift of the Yucatan Current position at the base of the LC, with a lag of 5–10 days. Furthermore, according to the authors, the presence of anticyclonic eddies in the northwestern Caribbean Sea coincides with retracted LC phases, whereas the absence of such eddies usually coincides with extended LC phases. Androulidakis et al. (2021) used Eulerian analysis on altimetry-derived data and drifter trajectories to identify anticyclonic eddies in the northwestern Caribbean Sea, as well as limited Lagrangian analysis using the “geodesic eddy detection”, a method to objectively detect coherent material eddies (Haller and Beron-Vera, 2013; Haller and Beron-Vera, 2014), which they applied on numerical model near-surface velocities. The geodesic eddy detection method identifies fluid regions with the same averaged material stretching (to the first order), that experience no filamentation under advection (Haller and Beron-Vera, 2013; Haller and Beron-Vera, 2014). Their results confirmed that surface anticyclonic relative vorticity flux at the Yucatan Channel is present mostly during retracted LC phases. We here aim to expand on these findings, by performing a different Lagrangian analysis, based on vorticity, the “Lagrangian-Averaged Vorticity Deviation” (LAVD, Haller et al., 2016), that was used in Androulidakis et al. (2021) to identify near-surface coherence of only one particular Caribbean Anticyclone (CarA). LAVD, unlike the geodesic method, is associated with regions of high vorticity and tangential boundary filamentation is allowed. In the present study, LAVD is applied on model velocities in the entire water column, to identify eddies south of the Yucatan Channel.

The anticyclonic Caribbean eddies were first mentioned in Murphy et al. (1999), who performed a modeling study on the connectivity of the mesoscale field among the Caribbean Sea, the GoM, and the Atlantic Ocean. The authors argued that there is statistically significant correlation between eddies that form in the easternmost Caribbean Sea and the LCE shedding events. They also noticed interactions between the anticyclonic Caribbean eddies and the LC main body, after the Caribbean eddies enter the GoM through the Yucatan Channel. The concept of connectivity between the tropical Atlantic Ocean and the GoM was also discussed in the

recent study by Huang et al. (2021). The authors, using satellite products of altimetry, sea surface salinity, and chlorophyll, argued that freshwater from the tropical Atlantic can be transported to the GoM through mesoscale features that travel through the Lesser Antilles to the Caribbean Sea. The freshwater input from the tropical Atlantic can impact the variability of the GoM dynamics, adding to the complexity of the system (Huang et al., 2021). Oey et al. (2003) in their modeling study, using Eulerian estimates, suggested that the LCE shedding cycles are subject to wind-induced transport fluctuations of the Yucatan Current and the presence of anticyclonic eddies originating in the Caribbean Sea. More specifically, they showed that anticyclonic activity in the northwestern Caribbean Sea promotes longer LCE shedding intervals, while wind-induced transport fluctuations are connected to shorter LCE shedding intervals. Garcia-Jove et al. (2016), in their modeling study, showed that Caribbean anticyclones are associated with LCE detachments but noted that they are not the primary driver of the detachments. Instead, the authors argue that instabilities that take place in the Campeche Bank and the LC extension are the primary mechanism for LCE detachments and/or final separations. However, Athié et al. (2012) argued that another factor connected to the LC evolution and LCE shedding is the eastward shift of the Yucatan Current, caused by cyclonic eddies generated south of the Yucatan Current, right before LCE detachments. Candela et al. (2002), using data from a mooring array of Acoustic Doppler Current Profilers (ADCPs) across the Yucatan Channel, calculated the potential vorticity flux that enters the GoM and concluded that LCE shedding events follow periods of cyclonic vorticity flux at the Yucatan Channel. Gopalakrishnan et al. (2013) also showed that LCE separations are associated with cyclonic vorticity at the YC and frontal eddy intensification on the eastern side of the LC. Following the study by Candela et al. (2002); Oey (2004) also studied the Eulerian vorticity flux through the Yucatan Channel with respect to LC variability, using both observations across the Yucatan Channel, satellite SSH, and model simulations. Based on their results, conversely to Candela et al. (2002), anticyclonic vorticity flux at the Yucatan Channel triggers LCE shedding events or promotes retracted LC phases.

The variability of the LC has also been studied with respect to transport at the Yucatan Channel. Lin et al. (2009) in their modeling study, argued that the maximum vertically integrated transport occurs during retracted LC phases, particularly after LCE shedding events, whereas the minimum values occur during extended LC phases. Focusing on the deep flow in the Yucatan Channel, Bunge et al. (2002) found that the deep transport at the Yucatan Channel is correlated with both the LC northern extension and the expansion of the LC area, suggesting that the Yucatan Undercurrent might also contribute to the LC variability. Similarly to Athié et al. (2012); Sheinbaum et al. (2016) found that eastward shifts of the Yucatan Current core are related to vorticity perturbations originating in the Caribbean Sea and are evident before LCE detachments. However, they claim that such connections are not always apparent, as there are other factors that influence the variability of the LC and the LCE shedding cycles. They also tried to establish a correlation between the transport at the Yucatan Channel and the vorticity fluctuations from the Caribbean Sea, but this was inconclusive due to the high variability of the Yucatan current system and the limited amount of available data. Furthermore, Abascal et al. (2003), based on

observations at the Yucatan Channel, showed that the variability of the flow at the Yucatan Channel is mostly governed by both anticyclonic and cyclonic eddies.

Overall, the dynamics of the LC evolution that are governed by processes at the Yucatan Channel as well as the Caribbean Sea and the GoM cannot be explained based on a specific mechanism. Many processes can be simultaneously responsible for the variability of the LC system, such as the meteorological conditions of the region, eddy activity, fluctuations in the Yucatan transport, both in upper and deeper layers, through shifts of the Yucatan Current, and vorticity perturbations in the two basins as well as across the Yucatan Channel (Athié et al., 2020).

The main objective of this study is to focus on one process, specifically to investigate the effects of the mesoscale activity upstream of the Yucatan Channel (northwestern Caribbean Sea) on the LC system evolution, expanding on the findings by Androulidakis et al. (2021). This is done using a robust Lagrangian eddy detection methodology that identifies vortices objectively based on the vorticity of the fluid mass (Haller et al., 2016). We will discuss the LC dynamics with respect to vorticity fluxes at the Yucatan Channel, which are attributed to coherent eddies that originate in the Caribbean Sea in tandem with the LC variability, using a 7-year period of model data. We will also focus on individual case studies of detected coherent eddies that coincide with both retracted and extended LC phases, to explore how the connectivity between the two basins is associated with the LC evolution and coherent Caribbean eddies variability.

The model configuration and the eddy-tracking methodology are presented in Section 2. The results are included in Section 3. A brief concluding summary is provided in Section 4.

2 Methodology

2.1 Model description

The numerical simulation output data are obtained from the Hybrid Coordinate Ocean Model (HYCOM; hycom.org; Bleck, 2002; Halliwell, 2004). The model domain covers the north Atlantic, the Gulf of Mexico, and the Caribbean Sea from 98° W to 20° W and from 5° S to 45° N (Figure 1A), at 1/25° horizontal resolution and 35 hybrid vertical layers (ATL-HYCOM 1/25). Depending on the topographic characteristics and the vertical structure, the hybrid vertical coordinates are optimized to best represent the ocean dynamics of the area. The distribution of the vertical coordinates is isobaric in the mixed layer and in very shallow areas, terrain-following at the continental shelf, and isopycnal in the stratified ocean interior (Bleck, 2002). The current configuration (ATL-HYCOM 1/25) uses initial and boundary conditions from the Global HYCOM (GLB-HYCOM), at 1/12° horizontal grid resolution and 32 hybrid vertical layers (Androulidakis et al., 2016). The atmospheric forcing is obtained from the Navy Operational Global Atmospheric Prediction System (NOGAPS) and the Navy Global Environmental Model (NAVGEM). The model performance was evaluated in Androulidakis et al. (2016) and Kourafalou et al. (2016) who showed good agreement between the model output and *in situ* and satellite observations. ATL-HYCOM 1/25 has also served as a Nature

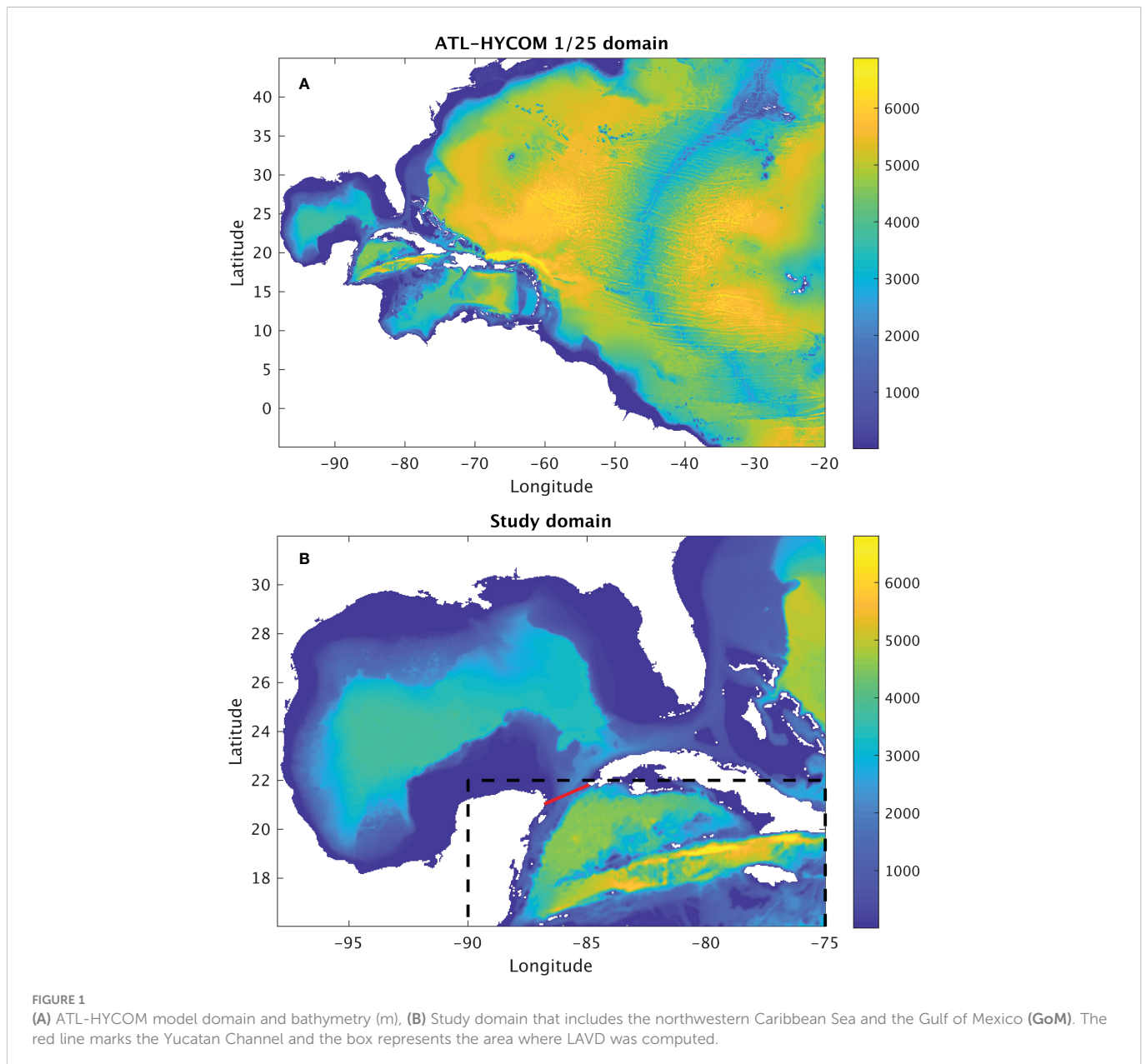
Run for Observing System Simulation Experiments OSSEs, designed to improve model skill, and was further evaluated in Halliwell et al. (2017). The configuration is free-running (no data assimilation) and appropriate for the process-oriented purposes of this study. Furthermore, since the model domain covers both the Caribbean Sea and the GoM, it is suitable for analyzing processes that take place in both regions as well as inter-basin exchanges (Androulidakis et al., 2021). For our analysis, we focus on a 7-year period (2010-2016) to investigate the relationship between the mesoscale eddy variability in the northwestern Caribbean Sea and the LC evolution.

2.2 Detection of coherent eddies

In our Lagrangian analysis, we aim to detect eddy structures in the Caribbean Sea that pass through the Yucatan Channel, interacting with the predominant mesoscale features in the GoM. We employ an eddy-detecting methodology, the Lagrangian-Averaged Vorticity Deviation (LAVD), developed by Haller et al. (2016), who defined Lagrangian rotationally coherent vortices from relative vorticity. As vortices are often considered regions of vorticity maxima or minima (Haller, 2005; Haller et al., 2016), efforts have been made toward defining a vortex based on that property. Haller (2005) reviewed such definitions, according to which vortices are characterized by closed streamlines that remain invariant under Galilean transformations, such as the *Q-criterion* (Hunt et al., 1988), the *Okubo-Weiss criterion* (Okubo, 1970; Weiss, 1991), and the λ_2 -*criterion* (Jeong and Hussain, 1995). However, these criteria do not remain invariant under rotational transformations, hence the notion of objectivity, which is necessary for a generalized vortex definition, is not satisfied. Objectivity is achieved when vortices remain the same under transformations to different frames of reference (Haller, 2005). Haller et al. (2016) overcame the difficulties of defining coherent vortices from vorticity, mainly the lack of objectivity, and showed that even though vorticity is not objective, meaning that the vorticity tensor is not invariant under changes of observers, the LAVD is, in fact, an objective field. The LAVD is defined as:

$$LAVD_{t_0}^{t_0+T}(x_0) := \int_{t_0}^{t_0+T} |\omega(F_{t_0}^t(x_0), t) - \bar{\omega}(t)| dt \quad (1)$$

where ω is the relative vorticity, $\bar{\omega}$ the spatial mean relative vorticity, and $F_{t_0}^t(x_0)$ is the flow map, which is defined as the mapping from the initial position x_0 at time t_0 to some later position $x(t; x_0, t_0)$ at time $t = t_0 + T$. According to the LAVD-based definition, the centers of rotationally coherent vortices are characterized by local LAVD maxima and the boundaries are the outermost closed convex level surfaces of LAVD. Each LAVD level set is composed of fluid particles that complete the same total material rotation relative to the mean material rotation of the whole fluid mass (Haller et al., 2016). This definition along with the objective nature of their detection method makes them robust indicators of the mesoscale eddy field in oceanic flows (Haller, 2005). Unlike geodesically detected eddies, eddies detected using the LAVD approach are allowed to experience filamentation. However, filamentation is observed to typically develop tangentially, without global breakaway. As it is based on vorticity, the method described by Haller et al. (2016) may be regarded as oceanographically more



appealing than the geodesic method, which produces similar results with some caveats, such as the sensitivity to parameters during computation (Andrade-Canto et al., 2020). Tarshish et al. (2018) expanded on this issue and focused on developing an index that classifies coherent structures detected using the LAVD method into three categories based on their coherency; strictly, moderately, and weakly coherent. Using different values for convexity deficiency, they calculated the mean and median coherency indices for the coherent structures detected based on a certain convexity deficiency. The large variation of their results supported their argument on the highly sensitive nature of the LAVD method regarding the tuning of the computational parameters.

However, despite the limitations, the LAVD method is considered a robust method to identify Lagrangian coherent eddies; the study by Beron-Vera et al. (2013), with the use of concrete examples, expanded on the advantages of using an observer-independent method for eddy detection as opposed to the classic SSH-based eddy detection.

Moreover, Liu et al. (2019), who quantified the material coherence of Eulerian SSH eddies and rotationally coherent Lagrangian vortices detected using the LAVD method, showed that SSH eddies are highly leaky and do not maintain their material coherence over the detection time interval, as opposed to the Lagrangian coherent vortices that were detected based on the LAVD method. They also showed that the SSH eddies may be coherent in their core, but they also may not, making SSH eddies almost indiscernible from any other body of water in the ocean, in terms of material coherence.

We applied the LAVD method in the northwestern Caribbean Sea (16° N - 22° N, 90° W - 75° W, Figure 1B) to assess eddy coherence during the study period, using the velocity fields from ATL-HYCOM 1/25, in each of the 35 layers of the model to allow for eddy detection at depth. In our calculations, the convexity deficiency was set at 10^{-2} . Lower convexity deficiency led to very few coherent eddies in the region of interest. According to the study by Tarshish et al. (2018), the value of the convexity deficiency chosen in the present study (10^{-2})

relates to coherency indices that indicate the identification of coherent structures that are not highly leaky. Although the authors developed their methodology based on outputs from a different numerical model, they argue that it should be applicable to data from other numerical models, as well. The LAVD is calculated every 15 days and integration time T was set to 15 days, a time period that is sufficient for detecting coherent mesoscale eddies using either observational or realistic model data (Beron-Vera et al., 2018; Androulidakis et al., 2021).

2.3 Advection of coherent boundaries and isopycnal particles

After coherence is established, the boundaries are advected to examine their pathways and physical connectivity with the GoM. The boundaries are advected as contour points using ODE45 in MATLAB and Dritschel's curvature interpolation (Dritschel, 1988). We will be using the term "boundary" for individual coherent contours and the term "eddy" when we refer to a group of boundaries in different layers that correspond to the same structure. Eddy coherence, using the LAVD method, has only been applied in fields from realistically forced, high-resolution model in Androulidakis et al. (2021), to examine the coherence and advection of anticyclonic Caribbean eddies (Caribbean anticyclones - CarAs) at the surface, as they approached the Yucatan Channel. The calculation of LAVD at depth using horizontal velocity fields at different layers from such a model to investigate eddy coherence throughout the entire water column is a novel approach, which to our knowledge, has not been applied in previous studies.

To better track the evolution of coherent structures, 2D Lagrangian particle experiments were also performed, with releases in two different layers either inside or in the vicinity of coherent boundaries. The particles were advected using the boundary advection method that is described in the previous paragraph.

2.4 Potential vorticity fluxes

We calculate potential vorticity (PV) fluxes at the Yucatan Channel attributed to coherent structures in the Caribbean Sea as an indicator of physical connectivity between the two basins. The potential vorticity is defined as:

$$PV = (fz + \nabla \times u) \cdot \nabla \left(-g \frac{\rho}{\rho_0} \right) = PV_1 PV_2 \quad (2)$$

where f is the Coriolis parameter, z is the unit vector of the z -coordinate, u is the velocity vector from which we take into consideration only the zonal and meridional components, g is the gravitational acceleration, ρ is the potential density, and ρ_0 is the reference density. The term PV_1 represents the absolute vorticity, and PV_2 represents the gradient of buoyancy. We compute the transport of PV (Φ) by rotationally coherent eddies as:

$$\Phi = \frac{\overline{PV}_\gamma A}{T} \quad (3)$$

where \overline{PV}_γ is the mean PV inside the coherent boundary, A is the area enclosed by the boundary, and T is the coherence time scale. This formula was also used by Androulidakis et al. (2021) to calculate surface relative vorticity fluxes of geodesic eddy boundaries (Haller and Beron-Vera, 2013; Haller and Beron-Vera, 2014). We will discuss the PV fluxes of all the boundaries that traverse through the Yucatan Channel and into the GoM. For our analysis we will only show the fluxes attributed to PV induced by horizontal shear, which is given by: $PV_{hshear} = -\frac{g}{\rho_0} \left(\frac{\partial v}{\partial x} - \frac{\partial u}{\partial y} \right) \frac{\partial \rho}{\partial z}$, a term derived from Eq. (2).

The PV induced by vertical shear is two orders of magnitude smaller than the horizontal shear induced PV and the planetary vorticity is unrelated to changes in the LC, as discussed by Candela et al. (2002), who calculated Eulerian PV fluxes based on velocity measurements at the Yucatan Channel.

3 Results

3.1 LC Variability and mesoscale eddy coherence in the Caribbean Sea

We examine eddy coherence in the northwestern Caribbean Sea with respect to LC evolution by only accounting for the coherent eddies that traverse through the Yucatan Channel (Figure 1B) upon 15 days of advection. Figure 2 shows the area of only the largest boundaries (diameter ≥ 90 km), normalized by the area of the largest boundary (A_{max}), that were detected south of the Yucatan Channel (Figure 1B) throughout the 7-year period along with the LC northern extension. Boundaries that are smaller than 90 km in diameter have been omitted for clarity. The dots that are assigned on the same dates usually represent parts of one eddy with coherent signature in multiple model layers, because an eddy with a coherent signature in various model layers consists of a group of coherent boundaries vertically. Thus, if multiple of these coherent boundaries have a

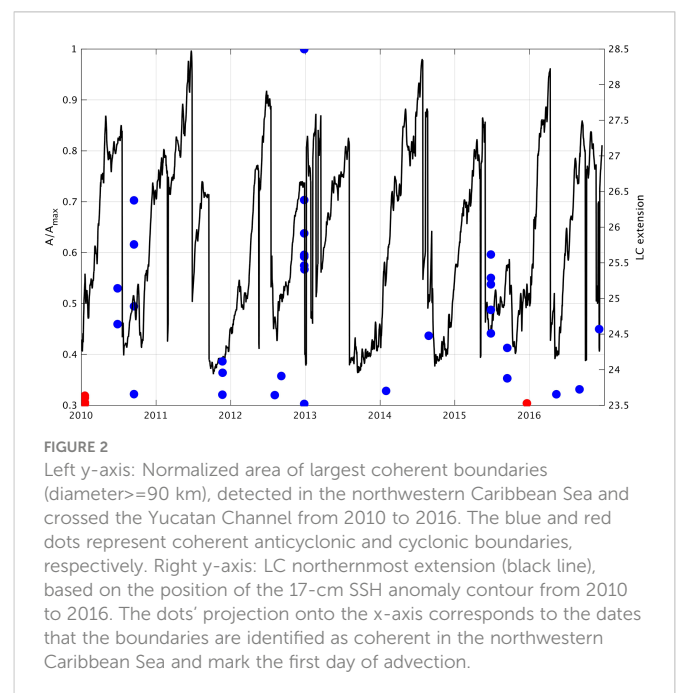


FIGURE 2
Left y-axis: Normalized area of largest coherent boundaries (diameter ≥ 90 km), detected in the northwestern Caribbean Sea and crossed the Yucatan Channel from 2010 to 2016. The blue and red dots represent coherent anticyclonic and cyclonic boundaries, respectively. Right y-axis: LC northernmost extension (black line), based on the position of the 17-cm SSH anomaly contour from 2010 to 2016. The dots' projection onto the x-axis corresponds to the dates that the boundaries are identified as coherent in the northwestern Caribbean Sea and mark the first day of advection.

diameter ≥ 90 km, they will represent a different dot on the same date. 86% of the coherent boundaries with diameter ≥ 90 km that are identified in the northwestern Caribbean Sea are anticyclonic, with the largest one reaching the diameter of 165 km. This boundary is part of an anticyclonic eddy that was identified as coherent in multiple layers of the model and was evident a few days before a LCE went through several detachments and reattachments prior to its final separation on August 2, 2013. Such pattern is evident in 50% of the detachments, in which anticyclonic coherent eddies with diameter ≥ 90 km were detected before LCE detachments or final separations (such as June 2010 and May 2016). In 70% of the instances where the LC was retracted, anticyclonic coherent boundaries with diameter ≥ 90 km are also evident (such as December 2011 and June 2015), while the cyclonic ones do not seem to follow a particular pattern.

Eddy coherence was evaluated throughout the entire water column (list of approximate layer depths in Table 1), and coherent boundaries were detected from layer 1 to layer 20 (≈ 650 m) (Figure 3A). No coherent boundaries were detected below layer 20 in the time period of 2010–2016. More specifically, more coherent anticyclonic boundaries than cyclonic ones were detected in all layers (up to layer 19) except for layer 20 where only a few cyclonic boundaries were detected (Figure 3A). The larger number of the coherent anticyclonic boundaries in all layers suggests that coherent anticyclonic eddies in the region are more likely to have a deeper signature than the cyclonic ones. However, overall, the polarity does not play a role on the depth to which the eddies can be detected, since both cyclonic and anticyclonic boundaries are present down to ≈ 650 m. Taking a closer look only at the boundaries with diameter ≥ 90 km, a total of 32 large anticyclones were detected (down to ~ 200 m), much higher than the total number of 4 cyclonic boundaries (down to ~ 100 m), throughout the 7-year period (Figure 3B). Such finding indicates that large coherent anticyclones are deeper and dominate the region in comparison with the cyclonic structures of equivalent size. The actual number of 3D eddies (grouping of boundaries at different layers with similar coordinates that represent parts of an individual eddy) is not calculated and would be outside of the scope of the study, since we do not focus on the number of eddies or boundaries but on the effect of the total volume and vorticity fluxes.

Figures 4A, B show the total anticyclonic volume in each of the 15-day period ($T = 15$ days: LAVD assessment period) of all the structures that were detected crossing the Yucatan Channel, down to layer 20 (≈ 650 m) and at surface, along with the LC extension, respectively. The discrete values of the anticyclonic volume of coherent boundaries are calculated at time t_0 in the entire water column (Figure 4A) and at surface (Figure 4B). The volume of each boundary is computed by multiplying the area of the boundary by the layer thickness. The total anticyclonic volume attributed to coherent boundaries at the surface is two orders of magnitude smaller than the respective volume of coherent boundaries down to layer 20, with the pattern being similar in both cases (Figures 4A, B). However, coherence assessment in the entire water column provides a more comprehensive picture on the presence of LAVD vortices and their interaction with the LC system, since detection in the surface layer accounts for about 50% of the total flux occurrences. Thus, coherent boundaries that represent coherent eddies may appear at depths below the surface and would be unaccounted for if only the surface

TABLE 1 List of approximate layer depth ranges for the region south of the Yucatan Channel and north of 18 N.

Layer#	Depth(m)
1	~2
2	~6
3	~12
4	~30
5	~40
6	~40
7	~70-100
8	~100-150
9	~150-200
10	~200
11	~200-250
12	~250-300
13	~300-350
14	~350-400
15	~400-450
16	~450-500
17	~500-550
18	~550-600
19	~600-650
20	~650-800
21	~800-900
22	~900-950
23	~950-1000
24	~1000-1100
25	~1100-1200
26	~1200-1300
27	~1300-1500
28	~1500-2000
29	~2000-3500
30	~3500-4000
31	~4000-4500
32	~4000-4500
33	~4000-4500
34	~4000-4500
35	~4000-4500

circulation was analyzed. However, it should be noted that the presence of noise in the surface layer can contribute to a failure in the LAVD method to identify vortices, hence the lower number of coherent boundaries detected in layer 1.

Focusing on the at-depth coherence assessment, the largest values of anticyclonic volume ($\geq 10^6$ m³) are mostly evident when the LC is

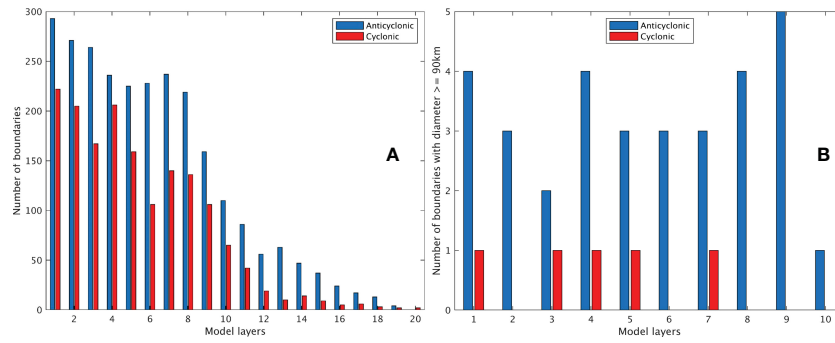


FIGURE 3 (A) Total number of anticyclonic (blue) and cyclonic (red) boundaries in each model layer (layers 1-20; ~650m), detected in the northwestern Caribbean and passed through the Yucatan Channel and (B) similar to (A) but for boundaries with diameter ≥ 90 km that are detected in model layers 1-10 (layer 10~200m).

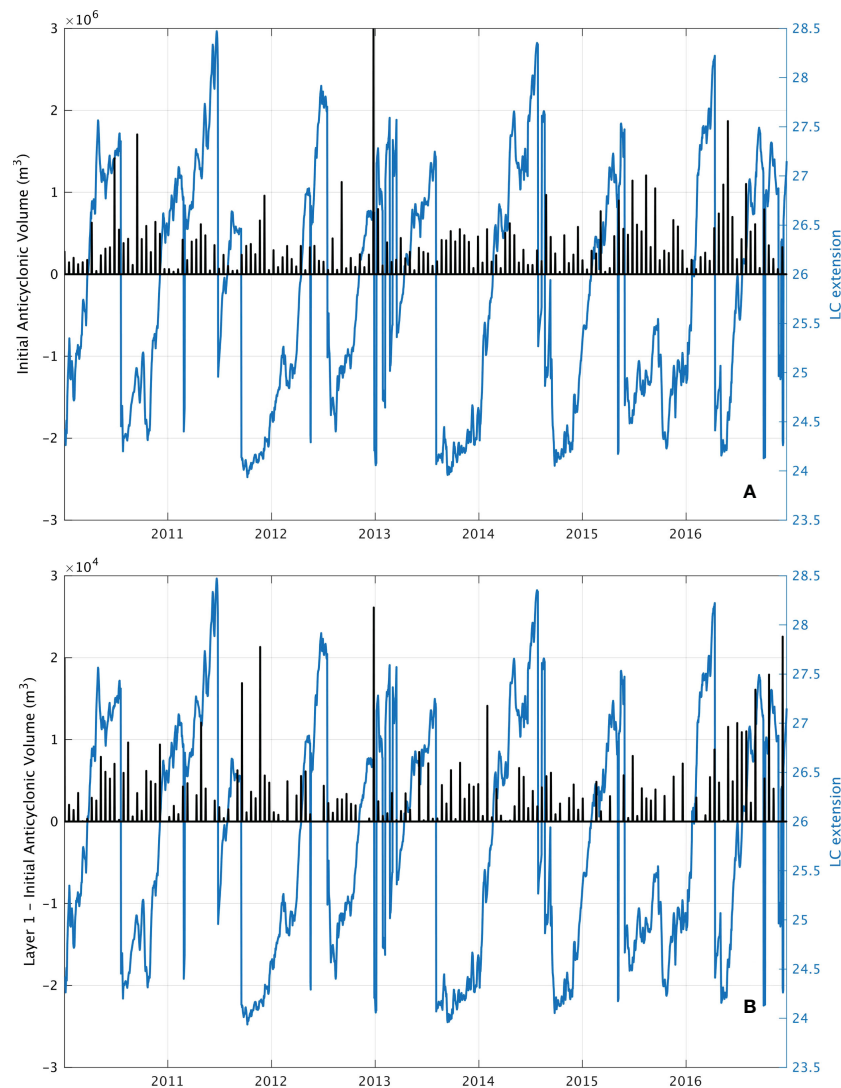


FIGURE 4 Initial volume of anticyclonic, coherent boundaries (black bars) that were detected in the northwestern Caribbean Sea and crossed the Yucatan Channel (max total volume: 300 km^3), along with the LC northernmost extension (blue line) (A) in the entire water column and (B) at the surface.

retracted or before LCE detachments (Figure 4A), indicating that large coherent anticyclones are associated with retracted LC phases (Androulidakis et al., 2021). This finding is in agreement with the result presented in Figure 2, in which the normalized areas of the largest anticyclonic coherent boundaries are also associated to retracted LC phases. After grouping all the identified coherent boundaries based on their polarity, the anticyclonic eddies that cross the Yucatan Channel tend to also be larger than the cyclonic ones in terms of total initial volume (not shown). The 7-year mean coherent anticyclonic volume that originates in the northwestern Caribbean Sea and ends up being advected into the GoM is $\sim 20 \text{ km}^3$, whereas the mean cyclonic one is $\sim 13 \text{ km}^3$.

3.2 Potential vorticity fluxes through the Yucatan Channel

Figure 5 shows the discretized horizontal shear induced PV flux, calculated for every coherent boundary and summed over the total number of detected boundaries in all layers of the model that propagate into the GoM, along with the LC extension from 2010 to 2016. The PV flux is summed over the 20 layers of the model in which coherence was detected and it is computed within the boundaries that cross the red line in Figure 1B. The coherent PV flux values are normalized by the maximum value of the examination period. The largest coherent PV fluxes are anticyclonic (negative values) and, in 5 cases, intensified anticyclonic PV fluxes are evident before LCE detachments or final separations (such as June 2010 and December 2012, Figure 5). This suggests that the presence of anticyclonic eddies in the northwestern Caribbean Sea is connected to the LC evolution and more specifically to the LCE detachments or separations. Furthermore, large anticyclonic fluxes are evident during retracted LC phases (Figure 5) and along with the findings from Figure 4 indicate that the coherent anticyclonic activity in the northwestern Caribbean Sea promotes retracted LC phases, in agreement with Androulidakis et al. (2021). The Eulerian study by Oey et al. (2003) showed that anticyclonic activity in the Caribbean Sea is also associated with retracted LC phases, although a direct comparison to our results would not be optimal due to the lagrangian nature of our study. On the other hand, Candela et al. (2002), in their Eulerian study, showed that cyclonic vorticity flux is present before LCE detachments. In our study, there are a couple of cases (i.e., 2015, 2016) out of a total of 9, where cyclonic activity is pronounced right before the start of LCE shedding events (Figure 5). Nonetheless, the values are not as large as the largest anticyclonic vorticity flux values. However, larger cyclonic PV fluxes (>0.2) do occur in other instances (years 2013 and 2014) as well, when the LC is extended, about 45–50 days before LCE detachments/separations. This is a considerably larger time interval than the coherence assessment time interval selected in the present study (15 days), thus establishing a relationship between intensified cyclonic PV fluxes and LCE detachments is not trivial. The controversy in the results as well as the high variability of the system indicated that a statistical approach using a longer time series of data may be needed to further elucidate the relationship between the coherent eddy activity in the Caribbean and the LC evolution.

During extended LC phases, $\sim 35\%$ of the normalized coherent PV flux values are in the bin range between 0 and 0.1, indicating weak coherent mesoscale activity in the northwestern Caribbean (Figure 6). The rest of the occurrence frequencies during extended LC phases are equally distributed in positive and negative PV flux values, except for a 7% of increased negative PV flux values occurring only when the LC is extended (north of 26° N). This is possibly connected to intensified anticyclonic activity before LCE detachments, as presented in Figure 5. On the other hand, during retracted LC phases (south of 26° N), almost 70% of the coherent PV flux values are negative, a finding that agrees with Androulidakis et al. (2021), who argued that anticyclonic surface relative vorticity attributed to geodesic eddies was more pronounced when the LC is retracted.

3.3 Case studies of coherent eddies and 2D Lagrangian particle experiments

We now focus on specific case studies of coherent Caribbean anticyclones associated with different LC phases.

3.3.1 Coherent anticyclones during extended LC phases

It is shown that anticyclonic coherent PV fluxes are often present before LCE detachments or final separations (Figure 5). On June 26, 2010 (Figure 7), the increased anticyclonic PV flux is attributed to one coherent anticyclone with multilayer signature starting at the depth of $\sim 100 \text{ m}$ just south of the Yucatan Channel and extending down to the depth of 200 m (layers 7 ($\approx 70\text{--}100\text{m}$), 8 ($\approx 100\text{--}150\text{m}$), and 9 ($\approx 150\text{--}200\text{m}$)). This anticyclone is particularly large with area and diameter of $1.15 \times 10^4 \text{ km}^2$ and $\sim 120 \text{ km}$, respectively, in the uppermost layer (layer 7 in Figure 7). The size is decreasing from layer 7 to layer 9, with a total decrease of 89% of the initial area at layer 9 compared to layer 7.

We will be discussing the evolution of the anticyclonic boundary only in the uppermost layer, as all three detected boundaries evolve in a similar way. Figure 8 shows the evolution of the vortex

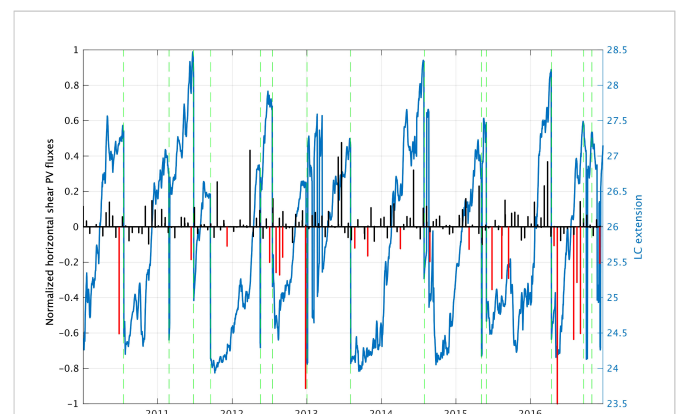


FIGURE 5
Normalized horizontal shear PV fluxes (black and red bars) of coherent boundaries detected south of the Yucatan Channel and propagated into the GoM, along with the LC northernmost extension (blue line). The red bars indicate values ≤ -0.1 . The dashed green lines mark the LCE detachments/final separations.

superimposed on SSH fields for up to 35 days from the day of detection (Jun 26, 2010, Figure 8A), along with the evolution of the LCE boundary (Figures 8A–D). After the coherent boundary enters the GoM, it quickly undergoes filamentation, exhibiting two pathways (July 15, 2010; Figure 8B). The first pathway wraps around the forming LCE, while part of the initial filament gets advected eastward, following the southern part of the LC towards the entrance of the Straits of Florida (Figure 8B). On July 20, 2010, the filament undergoes stretching, with its northern part continuously wrapping around the newly formed LCE (Figure 8C), until it is fully detached from the main LC body on July 30, 2010 (Figure 8D). Such evolution indicates that the coherent anticyclonic boundary detected south of the Yucatan Channel, contributes to the detached LCE, through the advection of anticyclonic Caribbean waters into the GoM. From an Eulerian point of view, Oey (2004) suggested that anticyclonic Potential Vorticity flux anomaly through the Yucatan Channel is associated with almost all the LCE shedding events in their 13-year modeling study period. However, the association of our findings with the results from Oey (2004) is not feasible, since Oey (2004) calculated the PV fluxes in the Eulerian sense along a line in the Yucatan Channel and we calculate PV fluxes from closed coherent eddy contours which were computed from a Lagrangian perspective.

The LCE was detected coherent by July 15, 2010 (Figure 8B). The coherent LCE undergoes some tangential filamentation on July 20, 2010 (Figure 8C), that further develops by July 30, with the boundary exhibiting more filamentation as time progresses (Figure 8D). Throughout this period, the boundary of the LCE encloses the high SSH values that indicate the presence of an anticyclonic eddy, objectively marking the boundaries of that eddy. These might differ from the traditional tracking of the LCE and LC boundaries, based on the 17-cm SSH contour anomaly, proposed by Leben (2005) (Beron-Vera et al., 2018; Andrade-Canto et al., 2020).

The above findings suggest that the anticyclonic Caribbean eddy enters the GoM and wraps around the newly detected coherent LCE. This suggests that the LCE formation is associated with the coherent

anticyclonic vorticity fluxes through the Yucatan Channel. To better elucidate the evolution of both coherent structures, we present Lagrangian particle experiments; 1250 isopycnic particles were released inside the Caribbean eddy in layer 7, located at the depth of approximately 70–100 m (layer of detection for both Caribbean anticyclone and LCE). In particular, the particles were released in the center of the Caribbean eddy, covering ~10% of the total boundary area (Figure 9A), and were advected for a total of 45 days. As shown in Figures 9B–D, the particles are advected northward along with the black contour and are finally traced inside the coherent boundary that marks the LCE (magenta colors). More specifically, 70% of the particles are found inside the LCE boundary from July 15, 2010 to August 9, 2010 (Figures 9B–D). The rest of the particles are still located within the black contour that originates in the coherent Caribbean anticyclone (Figures 9B, C). As a result, the particles that end up inside the LCE boundary outnumber the ones just outside of it, as shown in Figure 9E, that shows the positions of all 1250 particles in the 45-day period. Since the majority of the Caribbean waters originating in the core of the Caribbean anticyclone, represented by the Lagrangian particles, are advected into the LCE, it is suggested that in this case, the LCE detachment is facilitated by an anticyclonic incoherent filament originating from a coherent Caribbean anticyclone present under an extended LC. Identical experiments were conducted in layers 8 and 9 (~150–200m), where both the Caribbean anticyclone and the LCE were detected coherent and exhibited similar results in terms of the evolution of their boundaries, as well the percentage of particles that were traced inside the LCE after being released in the center of the Caribbean anticyclone (not shown). The process of a coherent eddy originating in a non-coherent filament is discussed in Wang et al. (2015), who showed that material vortices in the Agulhas region are formed by mostly south Atlantic incoherent water and then traverse through the subtropical gyre. In our case, the incoherent water tracked by isopycnal particles (Figures 9A–D) may partially originate in the coherent Caribbean anticyclone that underwent filamentation after

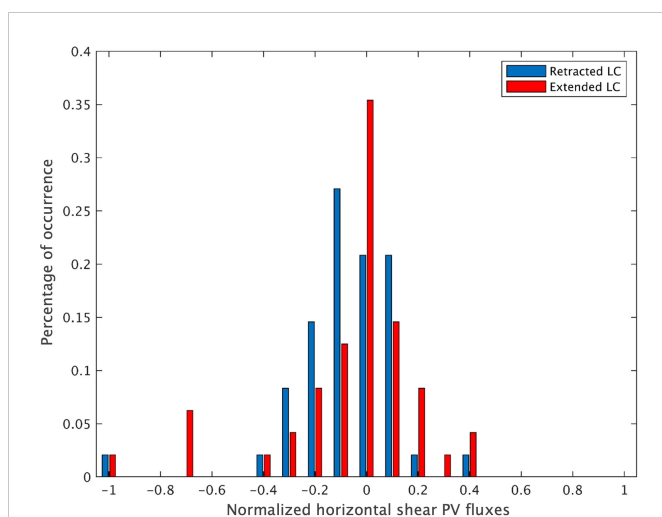


FIGURE 6 Occurrence frequencies of the PV fluxes (%) presented in Figure 5 for retracted (blue) and extended (red) LC phases.

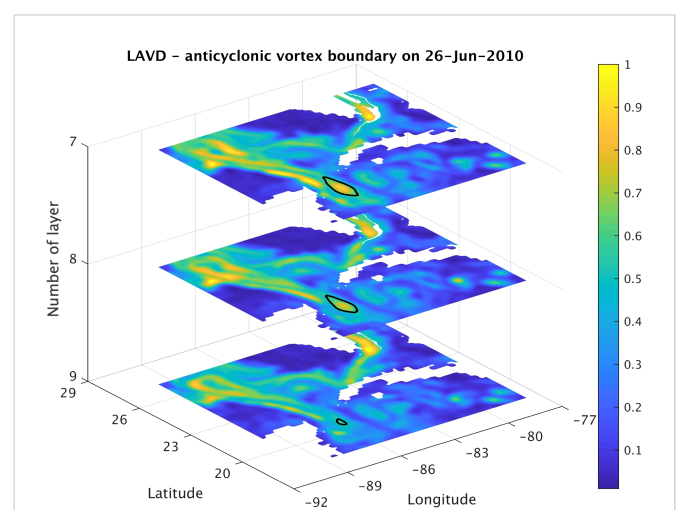


FIGURE 7 Coherent anticyclonic boundary (black) superimposed on the normalized LAVD field in model layers 7, 8, and 9 on June 26, 2010.

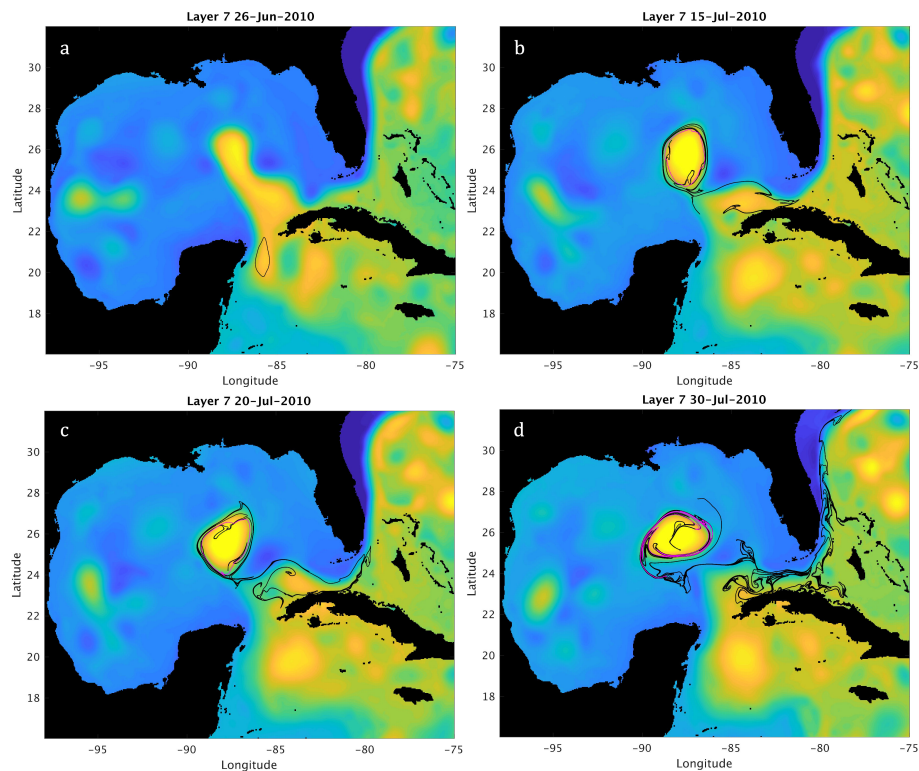


FIGURE 8

Snapshots of the evolution of the LCE boundary (magenta contours) and coherent anticyclonic boundary (black contours) detected south of the Yucatan Channel along with the, superimposed on model SSH for (A) June 26, 2010; day of coherent Caribbean anticyclonic boundary detection, (B) July 15, 2010; just after the LCE was detected coherent (magenta contours), and (C, D) 5 and 15 days later, respectively.

entering the GoM. However, this hypothesis needs further testing by advecting of the coherent LCE contour (Figure 8B) backward in time.

Neighboring seeding locations were also tested, to quantify the connectivity between the surrounding Caribbean waters and the LCE (Figures 10A, C, E). 1250 particles were released east of the anticyclonic boundary (Figure 10A), 2000 along the Yucatan Strait (Figure 10C), and 1000 particles on the eastern part of the Yucatan Strait (Figure 10E). All particles were advected for 45 days and their evolution from the day of each deployment until the advection end day, for each one of the different locations is shown in Figures 10B, D, F respectively. In the experiments presented in Figures 10A, E about 10% of the initial number of particles were traced in the LCE boundary, exhibiting weaker connectivity compared to the seeding case inside the core of the Caribbean anticyclone (Figure 9A), in which the equivalent percentage was 70%. Even weaker connectivity is suggested by the experiment presented in Figure 10C, where only 5% of the particles end up in the LCE contour. The particles that did not end up in the LCE boundary (Figures 10B, D, F), either recirculate in the northwestern Caribbean Sea, with the most intense recirculation being evident in Figure 10A, or are advected in the southeastern (Figures 10B, D, F) and northern GoM (Figure 10F), before exiting toward the Atlantic Ocean. The recirculation in the Caribbean Sea is not evident in the experiment presented in Figure 9, supporting the hypothesis of stronger connectivity between the core of the coherent Caribbean anticyclone and the newly formed LCE before this detachment event.

3.3.2 Coherent anticyclones during retracted LC phases

Intensified anticyclonic PV is also evident during retracted LC phases (Figure 5), in agreement with Androulidakis et al. (2021), where surface anticyclonic relative vorticity was calculated, based on geodesic eddies (Haller and Beron-Vera, 2013; Haller and Beron-Vera, 2014) detected in the Caribbean Sea. We now examine a case study of a coherent anticyclone present just south of the Yucatan Channel on June 24, 2015 (Figure 11). The anticyclone is detected coherent down to layer 12 ($\approx 250\text{--}300\text{m}$), starting from the layer 2, as shown in Figure 11. The area of the boundaries, marking the outermost part of the eddy, decreases with depth by 90% of the maximum value, except for a small increase of 7% from layer 2 to layer 3. The diameter of the eddy decreases from $\sim 122\text{km}$ at layer 2, to just 18km at the depth down to which an anticyclonic coherent boundary is present.

The evolution of the anticyclonic boundary in layer 2 (the uppermost layer where the anticyclone was detected coherent) is shown in Figure 12 and is quite different from the case study of an extended LC (Section 3.3.1). The LAVD vortex (Figure 12A) transforms into a non-coherent filament (Figure 12B), which undergoes stretching and more filamentation (Figure 12C) but is quickly advected in the Straits of Florida and the Atlantic Ocean (July 19, 2015, Figure 12D). Similar particle experiments to the ones presented in Figure 8 were performed for this case as well. More specifically, 1250 particles were released in the core of the anticyclone in layer 2 ($\sim 6\text{m}$). The particle-release experiment shows that all the

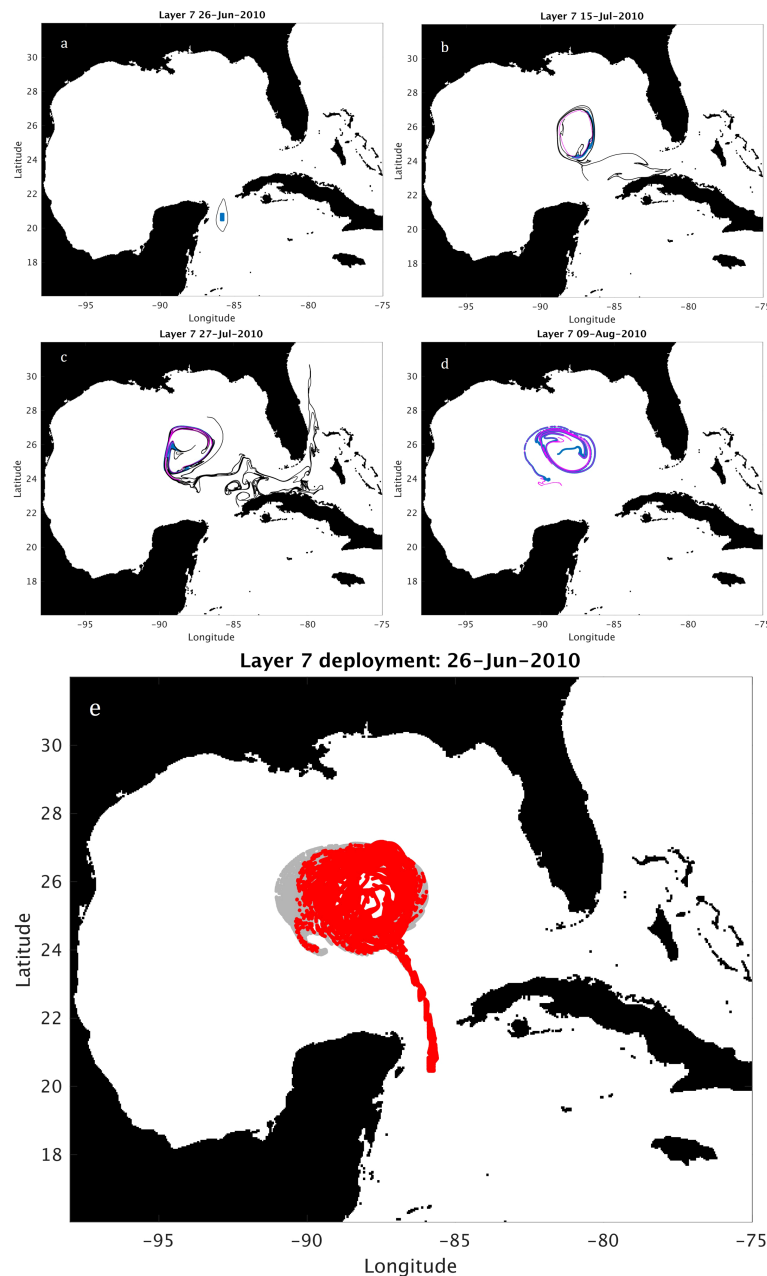


FIGURE 9
(A-D) Snapshots of Lagrangian particle advection, along with the evolution of both the Caribbean anticyclone (black contours) and the LCE boundary (magenta contours). **(E)** Particle evolution; the blue colors represent trajectories that were traced inside the LCE contour at the end of the 45-day experiment and the gray colors mark trajectories that were traced outside the LCE contour.

particles released in the core of the anticyclone (Figure 12A) are located east of 81°W on July 19 (Figure 12D), suggesting that these particles exit the GoM. The rapid advection of the coherent eddy while the LC is retracted is an indicator of strong physical connectivity between the Caribbean Sea and the Atlantic Ocean, conversely to the case presented in Figure 8, under an extended LC phase. While the LC is extended and before a LCE is detached from the main body, there is strong physical connectivity between the Caribbean Sea and the GoM, with most of the Caribbean waters (70% percent of total particles released) originating in the core of the

coherent Caribbean anticyclone being advected into the LCE. Our results agree with the study by Androulidakis et al. (2021), where the physical connectivity between the Caribbean Sea and the GoM was also studied by releasing Lagrangian particles in the northwestern Caribbean Sea. The authors note that during extended LC phases with no Caribbean anticyclonic eddy presence, the majority of the particles are advected in the GoM, whereas when the Caribbean anticyclones are present and the LC retracted, the majority of the particles is directly advected to the Atlantic Ocean, with only a small percentage of them reaching higher latitudes in the inner GoM. The authors also

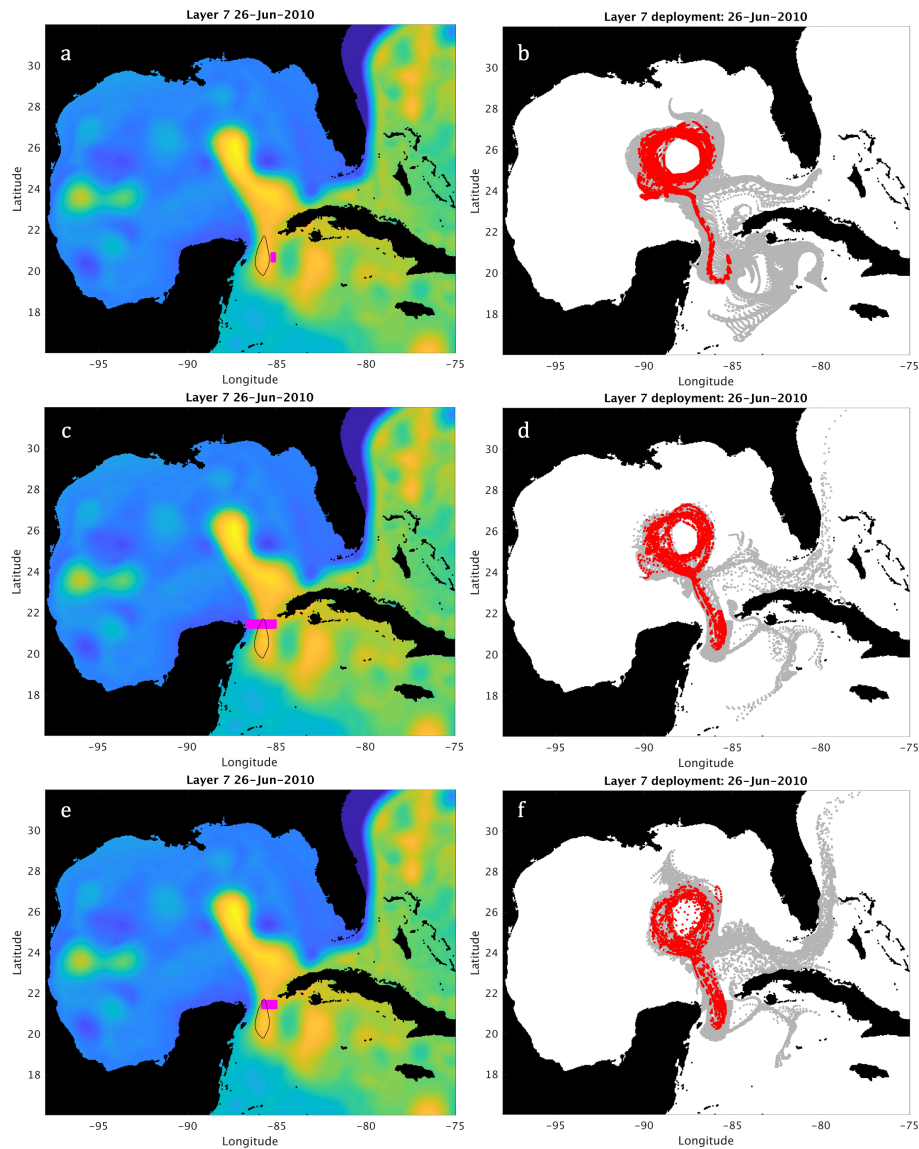


FIGURE 10

(A, C, E) Snapshots of seeding locations of Lagrangian particles (magenta boxes) and initial detection location of Caribbean anticyclone (black contour) superimposed on SSH. (B, D, F) Particle locations for each of the three particles experiments in panel (A, C, E), respectively. The red colors represent particles that were traced inside the LCE contour at the end of each 45-day experiment and the gray colors mark particles that were traced outside the LCE contour.

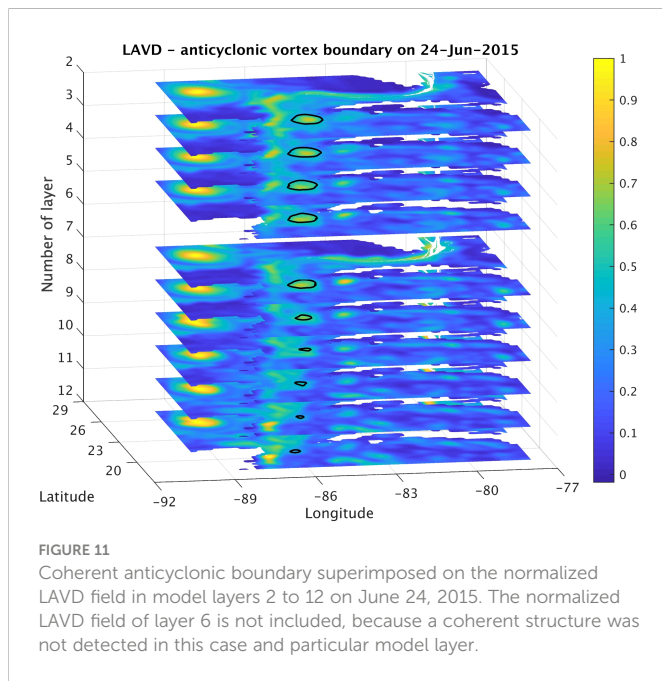
show the evolution of a coherent Caribbean anticyclone in the case of a retracted LC, in which the filament that originated in the coherent anticyclone traces another coherent vortex inside the retracted LC (Figure 11; Androulidakis et al., 2021).

Overall, our results show that the coherent eddy activity in the northwestern Caribbean Sea is associated with the LC phase transition and LCE shedding. More specifically, coherent anticyclonic fluxes that enter the GoM through the Yucatan Channel promote retracted LC phases, either by being evident during retracted LC phases or by facilitating LCE detachments and final separations. Coherent anticyclones with multi-layer signature in the Caribbean Sea can directly be associated with the water mass that

comprises a LCE or are indicators of physical connectivity between the Caribbean Sea and the Atlantic Ocean during retracted LC phases.

4 Summary and conclusions

We have evaluated eddy coherence in the Caribbean Sea and explored the interactions with extended and retracted LC phases, to assess the physical connectivity between the Caribbean Sea and the Gulf of Mexico (GoM), as well as processes that take place south of the Yucatan Channel, evolve through the channel, and influence the LC evolution.

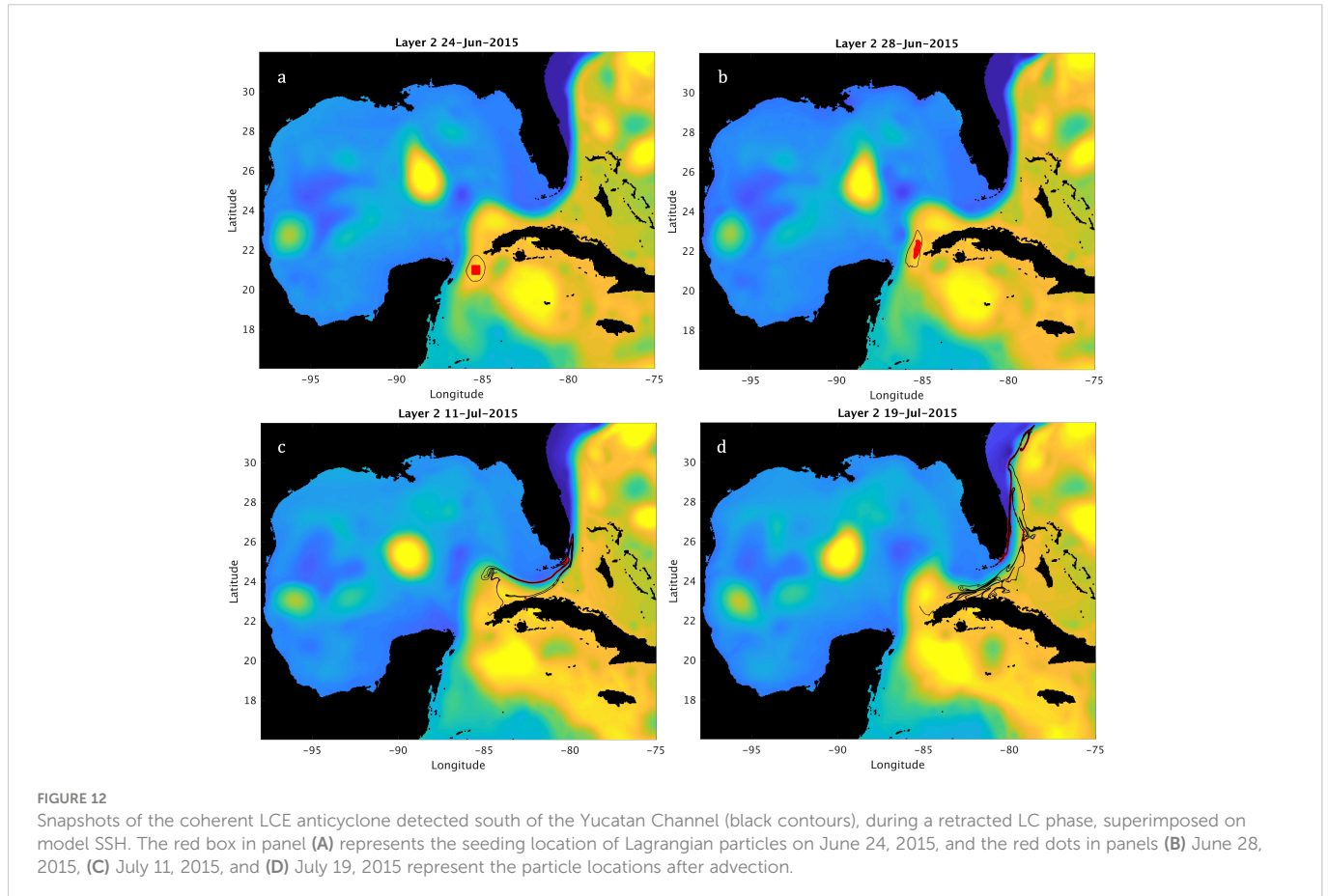


We approached the assessment of the mesoscale eddy field by applying the Lagrangian-Averaged Vorticity Deviation (LAVD) method for eddy identification, based on the relative vorticity of the fluid mass, a robust method for objectively identifying coherent eddy

centers and boundaries (Haller et al., 2016). Eddy coherence was assessed throughout the entire water column for a 7-year period (2010–2016), using the velocity fields from the high-resolution, free-running ATL-HYCOM 1/25. The identified eddy boundaries were then advected forward in time and their evolution is examined. As the purpose of this study is to investigate the inter-basin exchanges between the Caribbean Sea and the GoM, only the boundaries that pass through the Yucatan Channel were included in the analysis.

Eddies were detected in the northwestern Caribbean Sea over the upper $\approx 650\text{m}$, while their polarity does not play a role on the depth to which either cyclones or anticyclones are detected. However, a larger number of anticyclonic boundaries was detected in the deeper layers, indicating that anticyclones are more coherent with depth than the cyclones, as in the upper layers.

We further calculated depth-integrated coherent PV fluxes from closed coherent eddy contours that traverse through the Yucatan Channel. Such calculations, based on a Lagrangian point of view, differ from calculating Eulerian PV fluxes from velocity data at the Yucatan Channel, as is common in Eulerian studies. Our results suggest that the depth-integrated coherent anticyclonic PV flux at the Yucatan Channel is associated with retracted LC phases. During extended LC phases the coherent anticyclonic activity in the Caribbean Sea is generally weak. However, the majority of the instances where depth-integrated coherent anticyclonic PV fluxes are evident during extended LC phases is prior to LCE detachments. This happens in 5 out of 9 cases within 15 days prior to the start of LCE shedding events, suggesting that



the presence of coherent Caribbean anticyclones may be linked to one of the mechanisms controlling the LC evolution.

Case studies during a retracted LC phase and during an extended LC phase (prior to LCE shedding) suggest that the physical connectivity between the Caribbean Sea and the GoM differs depending -among other factors- on the LC extension. In the case of a retracted LC, non-coherent filaments that originate in coherent anticyclones in the Caribbean Sea are quickly advected toward the Straits of Florida, indicating weak connectivity with the GoM interior.

While our findings generally agree with [Androulidakis et al. \(2021\)](#), who tied the presence of Caribbean anticyclones to retracted LC phases, our results further indicate that strong anticyclonic activity in the Caribbean Sea can also be present prior to LCE detachments. In particular, a case study from June 2010 showed that non-coherent anticyclonic filaments originating in a coherent Caribbean anticyclone trace the coherent LCE. Furthermore, isopycnal particles seeded in the core of the Caribbean anticyclone are mostly being advected in the core of the coherent LCE. Such event can lead to direct connectivity between the core of the Caribbean anticyclone and the formed LCE prior to its detachment from the main LC body. The anticyclonic filaments advected in the GoM can also be traced in other anticyclonic structures in the GoM, also known as Cuban Anticyclones (CubANs), located in the northern coast of Cuba ([Kourafalou et al., 2017](#)), a case also reported by [Androulidakis et al. \(2021\)](#). The physical connectivity between the Caribbean eddies and the LCEs that may travel throughout the GoM may also have significant biochemical implications, affecting the quality and ecological characteristics of remote offshore and coastal areas.

Overall, our findings suggest that the coherent eddy activity in the northwestern Caribbean Sea affects the GoM mesoscale dynamics. The complexity of the LC system, however, necessitates accounting for a wide range of mechanisms to fully elucidate the underlying dynamics and further work is needed to characterize the extent to which each mechanism contributes to the overall dynamics of the region.

Data availability statement

The raw data supporting the conclusions of this article will be made available by the authors, without undue reservation.

References

- Abascal, A. J., Sheinbaum, J., Candela, J., Ochoa, J., and Badan, A. (2003). Analysis of flow variability in the Yucatan channel. *J. Geophys. Res. Ocean.* 108, 1–18. doi: 10.1029/2003JC001922
- Andrade-Canto, F., Karrasch, D., and Beron-Vera, F. J. (2020). Genesis, evolution, and apocalypse of loop current rings. *Phys. Fluids* 32, 116603. doi: 10.1063/5.0030094
- Androulidakis, Y., Kourafalou, V., Halliwell, G., Le Hénaff, M., Kang, H., Mehari, M., et al. (2016). Hurricane interaction with the upper ocean in the Amazon-Orinoco plume region. *Ocean Dyn.* 66, 1559–1588. doi: 10.1007/s10236-016-0997-0
- Androulidakis, Y. S., Kourafalou, V. H., and Le Hénaff, M. (2014). Influence of frontal cyclone evolution on the 2009 (Ekman) and 2010 (Franklin) loop current eddy detachment events. *Ocean Sci.* 10, 947–965. doi: 10.5194/os-10-947-2014
- Androulidakis, Y., Kourafalou, V., Ollascoaga, M. J., Beron-Vera, F. J., Le Hénaff, M., Kang, H., et al. (2021). Impact of Caribbean anticyclones on loop current variability. *Ocean Dyn.* 71, 935–956. doi: 10.1007/s10236-021-01474-9
- Athié, G., Candela, J., Ochoa, J., and Sheinbaum, J. (2012). Impact of Caribbean cyclones on the detachment of loop current anticyclones. *J. Geophys. Res. Ocean.* 117, 1–16. doi: 10.1029/2011JC007090
- Athié, G., Sheinbaum, J., Candela, J., Ochoa, J., Pérez-Brunius, P., and Romero-Arteaga, A. (2020). Seasonal variability of the transport through the yucatan channel from observations. *J. Phys. Oceanogr.* 50, 343–360. doi: 10.1175/JPO-D-18-0269.1
- Beron-Vera, F. J., Ollascoaga, M. J., Wang, Y., Triñanes, J., and Pérez-Brunius, P. (2018). Enduring Lagrangian coherence of a loop current ring assessed using independent observations. *Sci. Rep.* 8, 1–12. doi: 10.1038/s41598-018-29582-5
- Beron-Vera, F. J., Wang, Y., Ollascoaga, M. J., Goni, G. J., and Haller, G. (2013). Objective detection of oceanic eddies and the agulhas leakage. *J. Phys. Oceanogr.* 43, 1426–1438. doi: 10.1175/JPO-D-12-0171.1
- Bleck, R. (2002). An oceanic general circulation model framed in hybrid isopycnal-Cartesian coordinates. *Ocean Model.* 4, 219. doi: 10.1016/S1463-5003(01)00017-8

Author contributions

NN designed the study, performed all the data analyses, all necessary calculations, and wrote the manuscript. FB-V contributed to the conception of the study and provided the LAVD code draft. VK provided the HYCOM data. VK, MO, and MLH contributed to the conception of the study and provided input throughout the process. YA provided input during the data analyses process. All authors contributed to the article and approved the submitted version.

Acknowledgments

This research was made possible by a grant from the National Academy of Sciences, Engineering, and Medicine (Gulf Research Program UGOS #2000011056). ML received partial support for work on this publication by NOAA/AOML and was supported in part under the auspices of the Cooperative Institute for Marine and Atmospheric Studies (CIMAS), a cooperative institute of the University of Miami and NOAA (agreement NA20OAR4320472). The authors also acknowledge partial financial support by Prof. Eric Chassignet (FSU) and the Center for Ocean-Atmospheric Prediction Studies (COAPS). We greatly appreciate the comments of two reviewers, which helped improve the manuscript.

Conflict of interest

The authors declare that the research was conducted in the absence of any commercial or financial relationships that could be construed as a potential conflict of interest.

Publisher's note

All claims expressed in this article are solely those of the authors and do not necessarily represent those of their affiliated organizations, or those of the publisher, the editors and the reviewers. Any product that may be evaluated in this article, or claim that may be made by its manufacturer, is not guaranteed or endorsed by the publisher.

- Bunge, L., Ochoa, J., Badan, A., Candela, J., and Sheinbaum, J. (2002). Deep flows in the Yucatan channel and their relation to changes in the loop current extension. *J. Geophys. Res. Ocean.* 107, 1–7. doi: 10.1029/2001JC001256
- Candela, J., Sheinbaum, J., Ochoa, J., Badan, A., and Leben, R. (2002). The potential vorticity flux through the Yucatan channel and the loop current in the gulf of Mexico. *Geophys. Res. Lett.* 29, 16-1-16–4. doi: 10.1029/2002GL015587
- Chérubin, L. M., Morel, Y., and Chassignet, E. P. (2006). Loop current ring shedding: The formation of cyclones and the effect of topography. *J. Phys. Oceanogr.* 36, 569–591. doi: 10.1175/JPO2871.1
- Donohue, K. A., Watts, D. R., Hamilton, P., Leben, R., and Kennelly, M. (2016). Loop current eddy formation and baroclinic instability. *Dyn. Atmos. Ocean.* 76, 195–216. doi: 10.1016/j.dynatmoce.2016.01.004
- Dritschel, D. G. (1988). Contour surgery: A topological reconnection scheme for extended integrations using contour dynamics. *J. Comput. Phys.* 77, 240–266. doi: 10.1016/0021-9991(88)90165-9
- García-Jové, M., Sheinbaum, J., and Jouanno, J. (2016). Sensitivity of loop current metrics and eddy detachments to different model configurations: The impact of topography and Caribbean perturbations. *Atmosfera* 29, 235–265. doi: 10.20937/ATM.2016.29.03.05
- Gopalakrishnan, G., Cornuelle, B. D., and Hoteit, I. (2013). Adjoint sensitivity studies of loop current and eddy shedding in the gulf of Mexico. *J. Geophys. Res. Ocean.* 118, 3315–3335. doi: 10.1002/jgrc.20240
- Haller, G. (2005). An objective definition of a vortex. *J. Fluid Mech.* 525, 1–26. doi: 10.1017/S0022112004002526
- Haller, G., and Beron-Vera, F. J. (2013). Coherent Lagrangian vortices: The black holes of turbulence. *J. Fluid Mech.* 731, 1–10. doi: 10.1017/jfm.2013.391
- Haller, G., and Beron-Vera, F. J. (2014). Addendum to “Coherent Lagrangian vortices: The black holes of turbulence”. *J. Fluid Mech.* 755, 1–4. doi: 10.1017/jfm.2014.441
- Haller, G., Hadjighasem, A., Farazmand, M., and Huhn, F. (2016). Defining coherent vortices objectively from the vorticity. *J. Fluid Mech.* 795, 136–173. doi: 10.1017/jfm.2016.151
- Halliwell, G. R. (2004). Evaluation of vertical coordinate and vertical mixing algorithms in the HYbrid-coordinate ocean model (HYCOM). *Ocean Model.* 7, 285–322. doi: 10.1016/j.ocemod.2003.10.002
- Halliwell, G. R., Mehari, M. F., Le Hénaff, M., Kourafalou, V. H., Androulidakis, I. S., Kang, H. S., et al. (2017). North Atlantic ocean OSSE system: Evaluation of operational ocean observing system components and supplemental seasonal observations for potentially improving tropical cyclone prediction in coupled systems. *J. Oper. Oceanogr.* 10, 154–175. doi: 10.1080/1755876X.2017.1322770
- Huang, M., Liang, X., Zhu, Y., Liu, Y., and Weisberg, R. H. (2021). Eddies connect the tropical Atlantic ocean and the gulf of Mexico. *Geophys. Res. Lett.* 48, 1–10. doi: 10.1029/2020GL091277
- Hunt, J. C. R., Wray, A., and Moin, P. (1988). Eddies, streams, and convergence zones in turbulent flows. *Cent. Turbul. Res. Proc. Summer Progr.* 193–208.
- Jeong, J., and Hussain, F. (1995). On the identification of a vortex. *J. Fluid Mechanics* 285, 69–94. doi: 10.1017/S0022112095000462
- Kourafalou, V. H., Androulidakis, Y. S., Halliwell, G. R., Kang, H. S., Mehari, M. M., Le Hénaff, M., et al. (2016). North Atlantic ocean OSSE system development: Nature run evaluation and application to hurricane interaction with the gulf stream. *Prog. Oceanogr.* 148, 1–25. doi: 10.1016/j.pocean.2016.09.001
- Kourafalou, V., Androulidakis, Y., Le Hénaff, M., and Kang, H. S. (2017). The dynamics of Cuba anticyclones (CubANs) and interaction with the loop Current/Florida current system. *J. Geophys. Res. Ocean.* 122, 7897–7923. doi: 10.1002/2017JC012928
- Leben, R. R. (2005). Altimeter-derived loop current metrics. *Geophys. Monogr. Ser.* 161, 181–201. doi: 10.1029/161GM15
- Le Hénaff, M., Kourafalou, V. H., Dussurget, R., and Lumpkin, R. (2014). Cyclonic activity in the eastern gulf of Mexico: Characterization from along-track altimetry and *in situ* drifter trajectories. *Prog. Oceanogr.* 120, 120–138. doi: 10.1016/j.pocean.2013.08.002
- Le Hénaff, M., Kourafalou, V. H., Morel, Y., and Srinivasan, A. (2012). Simulating the dynamics and intensification of cyclonic loop current frontal eddies in the gulf of Mexico. *J. Geophys. Res. Ocean.* 117, 1–20. doi: 10.1029/2011JC007279
- Lin, Y., Greatbatch, R. J., and Sheng, J. (2009). A model study of the vertically integrated transport variability through the Yucatan channel: Role of loop current evolution and flow compensation around Cuba. *J. Geophys. Res. Ocean.* 114, 1–14. doi: 10.1029/2008JC005199
- Liu, T., Abernathy, R., Sinha, A., and Chen, D. (2019). Quantifying eulerian eddy leakiness in an idealized model. *Journal of geophysical research: Oceans.* 124, 8869–8886. doi: 10.1029/2019JC015576
- Lugo-Fernández, A. (2007). Is the loop current a chaotic oscillator? *J. Phys. Oceanogr.* 37, 1455–1469. doi: 10.1175/JPO3066.1
- Murphy, S. J., Hurlburt, H. E., and O’Brien, J. J. (1999). The connectivity of eddy variability in the Caribbean Sea, the gulf of Mexico, and the Atlantic ocean. *J. Geophys. Res. Ocean.* 104, 1431–1453. doi: 10.1029/1998JC900010
- Oey, L. Y. (2004). Vorticity flux through the Yucatan channel and loop current variability in the gulf of Mexico. *J. Geophys. Res. C Ocean.* 109, 1–10. doi: 10.1029/2004JC002400
- Oey, L. Y., Lee, H. C., and Schmitz, W. J. (2003). Effects of winds and Caribbean eddies on the frequency of loop current eddy shedding: A numerical model study. *J. Geophys. Res. C Ocean.* 108, 22–21. doi: 10.1029/2002JC001698
- Okubo, A. (1970). Horizontal dispersion of floatable particles in the vicinity of velocity singularities such as convergences. *Deep. Res. Oceanogr. Abstr.* 17, 445–454.
- Schmitz, W. J. (2005). Cyclones and westward propagation in the shedding of anticyclonic rings from the loop current. *Geophys. Monogr. Ser.* 161, 241–261. doi: 10.1029/161GM18
- Sheinbaum, J., Athié, G., Candela, J., Ochoa, J., and Romero-Arteaga, A. (2016). Structure and variability of the Yucatan and loop currents along the slope and shelf break of the Yucatan channel and campeche bank. *Dyn. Atmos. Ocean.* 76, 217–239. doi: 10.1016/j.dynatmoce.2016.08.001
- Tarshish, N., Abernathy, R., Zhang, C., Dufour, C., Frenger, I., and Griffies, St. (2018). Identifying Lagrangian coherent vortices in a mesoscale ocean model. *Ocean Model.* 130, doi: 10.1016/j.ocemod.2018.07.001
- Vukovich, F. M., and Maul, G. A. (1985). Cyclonic eddies in the eastern Gulf of Mexico. *J. Phys. Oceanogr.* 15, 105–117. doi: 10.1175/1520-0485(1985)015<0105:CEITEG>2.0.CO;2
- Wang, Y., Olascoaga, M. J., and Beron-Vera, F. J. (2015). Coherent water transport across the south Atlantic. *Geophys. Res. Lett.* 42, 4072–4079. doi: 10.1002/2015GL064089
- Weiss, J. (1991). The dynamics of enstrophy transfer in two-dimensional hydrodynamics. *Phys. D Nonlinear Phenom.* 48, 273–294. doi: 10.1016/0167-2789(91)90088-Q